

Faceting control in core-shell GaN micropillars using selective epitaxy

Sergiy Krylyuk,^{1,2,a} Ratan Debnath,^{1,3} Heayoung P. Yoon,^{4,5}
 Matthew R. King,⁶ Jong-Yoon Ha,^{1,2} Baomei Wen,^{1,3} Abhishek Motayed,^{1,2}
 and Albert V. Davydov¹

¹*Materials Science and Engineering Division, National Institute of Standards and Technology, Gaithersburg, Maryland 20899, USA*

²*Institute for Research in Electronics and Applied Physics, University of Maryland, College Park, Maryland 20742, USA*

³*N5 Sensors, Inc., Rockville, Maryland 20852, USA*

⁴*Center for Nanoscale Science and Technology, National Institute of Standards and Technology, Gaithersburg, Maryland 20899, USA*

⁵*Maryland Nanocenter, University of Maryland, College Park, Maryland 20742, USA*

⁶*Northrop Grumman ES, Linthicum, Maryland 21090, USA*

(Received 15 July 2014; accepted 14 October 2014; published online 23 October 2014)

We report on the fabrication of large-area, vertically aligned GaN epitaxial core-shell micropillar arrays. The two-step process consists of inductively coupled plasma (ICP) etching of lithographically patterned GaN-on-Si substrate to produce an array of micropillars followed by selective growth of GaN shells over these pillars using Hydride Vapor Phase Epitaxy (HVPE). The most significant aspect of the study is the demonstration of the sidewall facet control in the shells, ranging from $\{1\bar{1}01\}$ semi-polar to $\{1\bar{1}00\}$ non-polar planes, by employing a post-ICP chemical etch and by tuning the HVPE growth temperature. Room-temperature photoluminescence, cathodoluminescence, and Raman scattering measurements reveal substantial reduction of parasitic yellow luminescence as well as strain-relaxation in the core-shell structures. In addition, X-ray diffraction indicates improved crystal quality after the shell formation. This study demonstrates the feasibility of selective epitaxy on micro-/nano-engineered templates for realizing high-quality GaN-on-Si devices. © 2014 Author(s). All article content, except where otherwise noted, is licensed under a Creative Commons Attribution 3.0 Unported License. [<http://dx.doi.org/10.1063/1.4899296>]

Three-dimensional GaN micro- and nanostructures have the potential to boost the performance of GaN-based electronic and optoelectronic devices due to lower defect density compared to conventional planar thin-film devices and possible reduction of detrimental spontaneous polarization effects. Selective area epitaxy (SAE) techniques used to fabricate such structures have significantly advanced in the past few years and impressive results have been demonstrated.¹ GaN columns or rods grown along the c-axis bounded by six $\{1\bar{1}00\}$ m-plane facets are especially attractive because InGa_xN quantum wells formed on these facets benefit from the absence of polarization fields.² Large arrays of GaN micro- and nanocolumns have been successfully grown by SAE using metal organic vapor phase epitaxy (MOVPE) and molecular beam epitaxy techniques.^{3,4} GaN core/shell hexagonal columns have also been realized by inductively coupled plasma (ICP) dry etching of GaN films followed by MOVPE overgrowth to recover the m-plane facets.^{5,6} Controlled wafer-scale GaN pillars overgrowth technology on Si substrates is essential for the next-generation of GaN-based devices including light-emitting diodes, transistors, and field-emitters.

Hydride Vapor Phase Epitaxy (HVPE) has been recently used to selectively form p-GaN shells on ICP-etched GaN-on-Si pillars with demonstration that HVPE overgrowth yields pyramids with

^aElectronic mail: sergiy.krylyuk@nist.gov



semi-polar $\{1\bar{1}01\}$ side facets regardless of pillar cross-sections or processing conditions.⁷ This paper demonstrates the use of a simple phosphoric acid (PA) etch of GaN-on-Si pillars before HVPE overgrowth that drastically alters the shells morphology, producing GaN shells with non-polar $\{1\bar{1}00\}$ sidewalls. X-ray diffraction (XRD), room-temperature photoluminescence (PL), cathodoluminescence (CL), and Raman spectroscopy measurements are conducted on the core-shell structures, with results indicating significant improvement in the crystal quality and optical properties as well as reduction of strain in the overgrown structures as compared to the initial epitaxial GaN film on Si substrate.

Si-doped 0.8 μm thick GaN (0001) films were grown in a commercial MOVPE reactor on n^+ -Si (111) substrates with ≈ 150 nm thick $\text{Al}_{1-x}\text{Ga}_x\text{N}$ buffer layers. To form an etch mask, a 30 nm thick SiN_x film was deposited using plasma-enhanced chemical vapor deposition followed by e-beam deposition of a Ti/Ni (50 nm/120 nm) bi-layer. The 500 $\mu\text{m} \times 500 \mu\text{m}$ arrays of circles with the diameters of 1 μm , 1.5 μm , and 2 μm and pitches between the circles from 8 μm to 18 μm were fabricated using deep UV lithography and metal lift-off. The patterns were etched in an ICP system using a $\text{Cl}_2/\text{N}_2/\text{Ar}$ gas mixture at 40 $^\circ\text{C}$ and 5 mTorr for 5 min. As a result, arrays of GaN-on-Si pillars shaped as truncated cones with $\approx 0.8 \mu\text{m}$ GaN on top of $\approx 0.6 \mu\text{m}$ Si were obtained. After the ICP etch, the metal mask was etched in a $\text{HF}:\text{HNO}_3:\text{H}_2\text{O}$ (1:1:10 by volume) solution followed by reactive ion etch (RIE) to remove the SiN_x layer. Some samples received an additional chemical etch in diluted phosphoric acid (85 wt.% $\text{H}_3\text{PO}_4:\text{H}_2\text{O}$, 1:1) at 130 $^\circ\text{C}$ for 2 min. Finally, all samples were cleaned using the Radio Corporation of America (RCA) protocol and dipped in diluted HF (1:10 by volume) for 30 s followed by rinsing in de-ionized water and drying in flowing nitrogen gas immediately before loading in the HVPE reactor.

Undoped GaN shells were epitaxially grown over the etched GaN pillars in a custom-built horizontal HVPE reactor. All overgrowth experiments were performed at 450 Torr reactor pressure and either 950 $^\circ\text{C}$ or 1000 $^\circ\text{C}$. The GaCl_x volatile precursor was formed by passing 10 sccm to 20 sccm (standard cubic centimeters per minute) of HCl over a boat with molten Ga at 700 $^\circ\text{C}$. Ammonia at 20 sccm–100 sccm was used as the group V precursor and nitrogen (5000 sccm) was the carrier gas. Before the growth, substrates were annealed at the growth temperature for 5 min in a NH_3/N_2 flow.

The samples were examined using a scanning electron microscope (SEM). A Rigaku Smart Lab 9 kW high-resolution x-ray diffractometer was used to evaluate crystalline quality of the GaN using rocking curve measurements.⁸ An integrated HORIBA Jobin Yvon's LabRAM 800HR bench-top system was used for PL (Kimmon He-Cd, 325 nm) and Raman spectroscopy (Laser Quantum DPSS, 532 nm) measurements, respectively. XRD, PL, and Raman spectra were collected from the whole arrays of pillars. Local CL spectra were obtained using a Czerny-Turner spectrometer with a CCD camera, where the photons were collected by a diamond-turned parabolic mirror and dispersed with a grating with a groove spacing of 150 lines/mm. All CL measurements were performed with a beam acceleration voltage of 5 kV at room temperature.

Figs. 1(a)–1(c) show GaN-on-Si pillars produced by ICP etching, hereinafter referred to as ICP-etched pillars. Tapered morphology and wavy sidewalls of the pillars are similar to those reported earlier.^{7,9} GaN pillars that are additionally etched in hot phosphoric acid, hereinafter denoted as PA-etched pillars, exhibit partially alleviated plasma induced damage to the sidewalls, evident in reduced undulations and the appearance of micro-steps and micro-facets (Fig. 1(d)). PA-etching does not produce defect-related etch pits on the top c-plane of the pillars, as has been reported for higher etching temperatures.¹⁰ Fig. 1(d) clearly indicates faster etching of the AlGa_xN buffer layer which could be due to its poor crystalline quality.¹¹ It could also be related to the fact that AlN can be etched in PA more efficiently than GaN.¹²

HVPE grown shells on ICP- and PA-etched pillars at 950 $^\circ\text{C}$ using 20 sccm HCl and 100 sccm NH_3 are compared in Figs. 2(a) and 2(b). Overgrowth of the ICP-etched pillars produced truncated hexagonal pyramids with semipolar $\{1\bar{1}01\}$ side facets. This morphology is typical for SAE growth by metalorganic chemical vapor deposition^{13,14} and was also reported in our previous paper.⁷ The pyramids also exhibit $\{1\bar{1}00\}$ facets at the base with randomly varying width across the array. For some pyramids, $\{1\bar{1}00\}$ m-plane facets extend down to the silicon substrate, as shown in Fig. 2(a) (broken white line). In contrast, HVPE overgrowth of PA-etched GaN pillars have produced strikingly different shells with the morphology of hexagonal pyramids with vertical $\{1\bar{1}00\}$ sidewalls

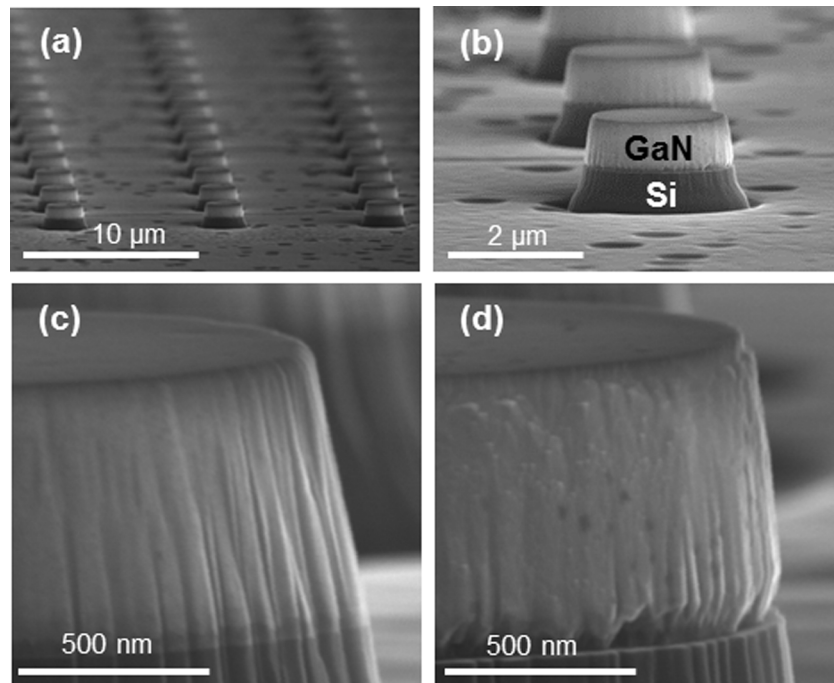


FIG. 1. SEM images of (a), (b) $2\ \mu\text{m}$ diameter GaN/Si pillars. (c), (d) Enlarged views of the pillar sidewalls after, (c) ICP etch and (d) additional phosphoric acid etch. Note microfaceting and reduced undulations in (d) compared to (c).

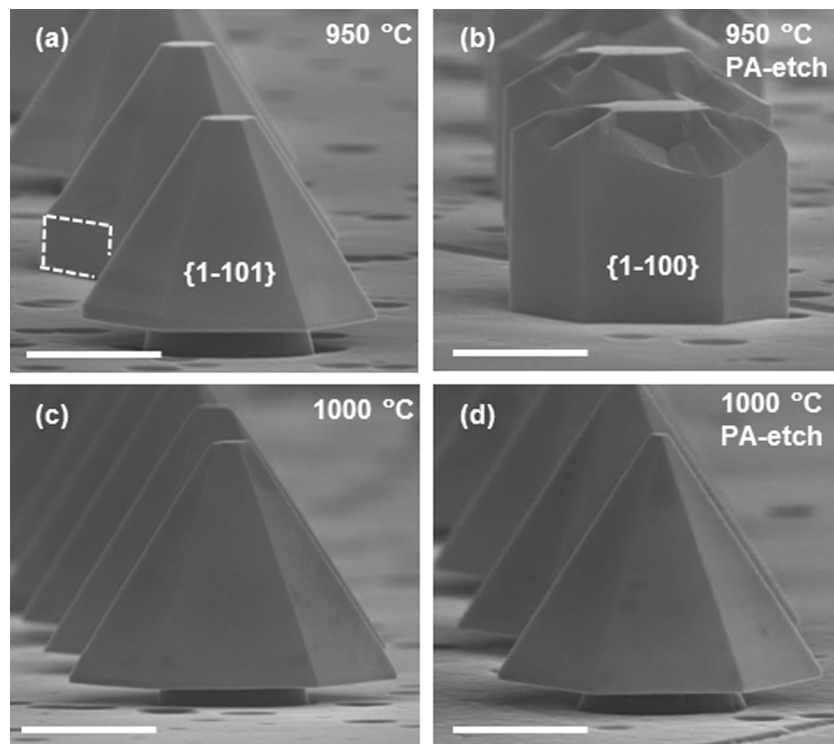


FIG. 2. GaN shells grown on $2\ \mu\text{m}$ diameter GaN/Si pillars for 2 min at (a), (b) $950\ ^\circ\text{C}$ and (c), (d) $1000\ ^\circ\text{C}$. Pillars used in (a) and (c) were ICP-etched only; those used in (b) and (d) were additionally etched in hot PA. White dashed line in (a) highlights one of the wide $\{1\bar{1}00\}$ facets that are observed on some pyramids. Scale bars correspond to $2\ \mu\text{m}$.

and wider (0001) top facet truncated by high-index vicinal facets (Fig. 2(b)). In addition, all shells appear to be in contact with the Si substrate. Their height is similar to that of the shells with inclined sidewalls grown over ICP-etched pillars, which implies the same, 850 nm/min, upward growth rate in the [0001] direction over both ICP- and PA-etched pillars. For comparison, the lateral growth rate in the $[1\bar{1}00]$ direction of the shells shown in Fig. 2(b) is about 400 nm/min. Low-magnification SEM images, shown in Fig. S1 of the supplementary material, illustrate the uniformity of the obtained core/shell structures across the array.¹⁵ Use of low V/III ratio is found to be effective for preventing spontaneous nucleation of GaN on the Si substrate, while low growth temperatures along with RCA cleaning and NH_3 annealing of the substrates prior to the HVPE growth have practically eliminated parasitic reactions between Si and Ga, known as “melt-back etching.”¹⁶

For the employed growth conditions, however, the impact of the PA-etching has disappeared at higher growth temperature. Figs. 2(c) and 2(d) show similar hexagonal pyramids with inclined $\{1\bar{1}01\}$ sidewalls for both ICP- and PA-etched pillars at 1000 °C growth temperature.

The ability to control sidewall polarity of the GaN core-shell structures by PA-etching of the GaN pillars is intriguing. In order to reveal mechanisms resulting in different faceting, shells are grown on ICP- and PA-etched pillars for 30 s to 6 min at the same pressure and temperatures as above but at a lower material deposition rate achieved by lowering HCl and NH_3 flows to 10 sccm and 20 sccm, respectively. The results are summarized in Fig. 3. For the ICP-etched pillars, growth starts on the top of the pillars forming (0001) and $\{1\bar{1}01\}$ facets. Besides, GaN nuclei that form on the sidewalls (Fig. 3(a)) eventually evolve into $\{1\bar{1}00\}$ facets as shown in Figures 3(b) and 3(e). Complimentary SEM images showing shell formation on ICP-etched pillars are given in Fig. S2. Essentially, initial stages of the shell growth are similar for the two temperatures. Overgrowth of ICP-etched pillars for 6 min at 950 °C and 1000 °C has yielded different shell morphologies

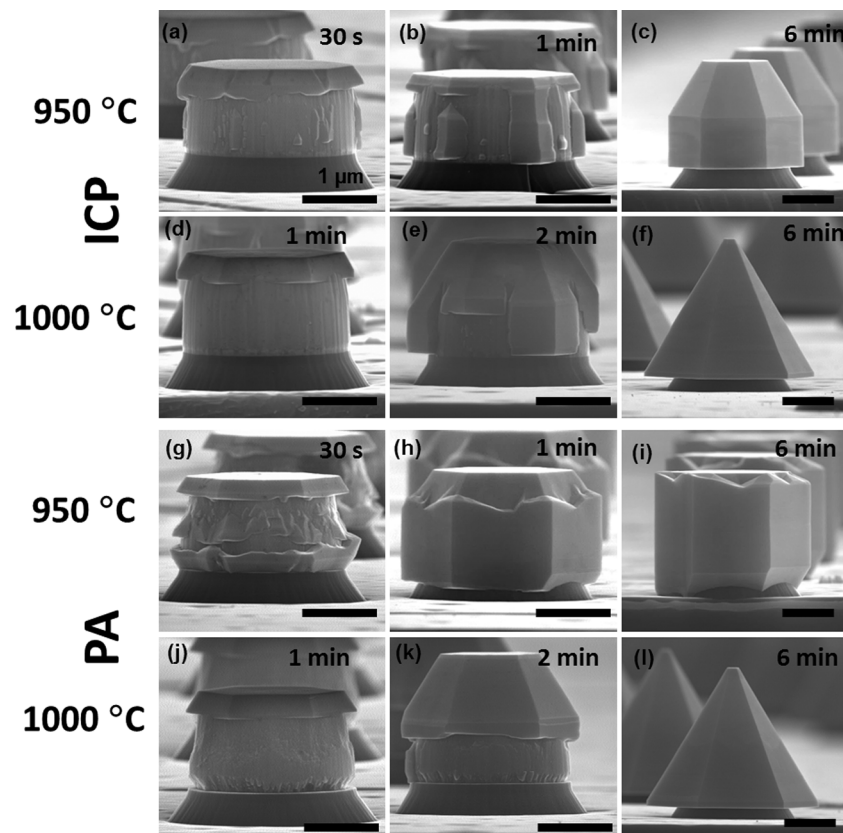


FIG. 3. GaN shells grown for different durations on (a)–(f) ICP- and (g)–(l) PA-etched pillars at 950 °C and 1000 °C. See text for details. Scale bars correspond to 1 μm .

(Figs. 3(c) and 3(f)). The shells grown at 950 °C exhibit well defined (0001) and $\{1\bar{1}00\}$ facets in addition to inclined $\{1\bar{1}01\}$ facets which dominate at higher $\text{GaCl}_x/\text{NH}_3$ flows as shown in Fig. 2(a). The pyramidal shells with $\{1\bar{1}01\}$ sidewalls were obtained at 1000 °C which resemble those shown in Fig. 2(c).

The initial stage of the shell growth on PA-etched pillars at 950 °C is depicted in Fig. 3(g); an enlarged view is given in Fig. S3. It is evident that the undercut at the Si-GaN interface created by faster etching of the AlGaN buffer layer provides an additional site for the GaN shell nucleation. Thus, two growth fronts that appear on the top and at the bottom of each pillar start moving toward each other. The facets formed by growth on the top of the pillars are (0001), $\{1\bar{1}01\}$, and $\{1\bar{1}00\}$, whereas the shell emerging from the bottom is bounded by $\{1\bar{1}00\}$ and presumably $\{1\bar{1}0\bar{1}\}$ planes. When the two growth fronts eventually merge, they define the shell morphology shown in Figs. 3(h) and 3(i). Notably, increasing the growth temperature eliminates nucleation at the bottom, in the vicinity of the AlGaN buffer. As a result, the shell growth proceeds similarly to the ICP-etched pillars (Figs. 3(j)–3(l)). Further experiments are underway to elucidate the underlying growth mechanisms.

Note, that despite the large difference in surface energies of $\{1\bar{1}01\}$ and $\{1\bar{1}00\}$ planes (dangling bond densities are 16.0 nm^{-2} and 12.1 nm^{-2} , respectively), they often co-exist for GaN columns produced in MOVPE as well as HVPE and SAE experiments.^{5,6,13,14} This implies that their growth is controlled by surface reaction kinetics so that variations in the growth environment can increase the relative deposition rate on one particular type of the facets, resulting in their disappearance, in accordance with the kinetic Wulff theory.¹⁷ Our preliminary experiments demonstrate that the resulting GaN shell morphology is, indeed, very sensitive to the local growth conditions. This is exemplified in Fig. S4, which shows shells with semipolar and non-polar sidewalls obtained on adjacent arrays of PA-etched GaN pillars with different pitches.

Structural and optical properties of individual core-shell pillars and their arrays are characterized using XRD, PL, Raman, and CL measurements. To limit the discussion, we present data only for the structures described in Figs. 2(a) and 2(b). Fig. 4 compares the GaN rocking curves of the (0002) reflection measured on the as-grown GaN epilayers vs. after the ICP etching (i.e., on etched pillars) and after the shell overgrowth (without and with PA-etch prior to the overgrowth). Table I summarizes the full-width half maximum (FWHM) values of the (0002) peak along with the peak intensity of all four samples. The large FWHM values for both thin-film and etched pillars indicated relatively poor GaN crystalline quality. The significant reduction of the FWHM value of the overgrown sample that received PA-etch prior to the overgrowth as compared to the other three

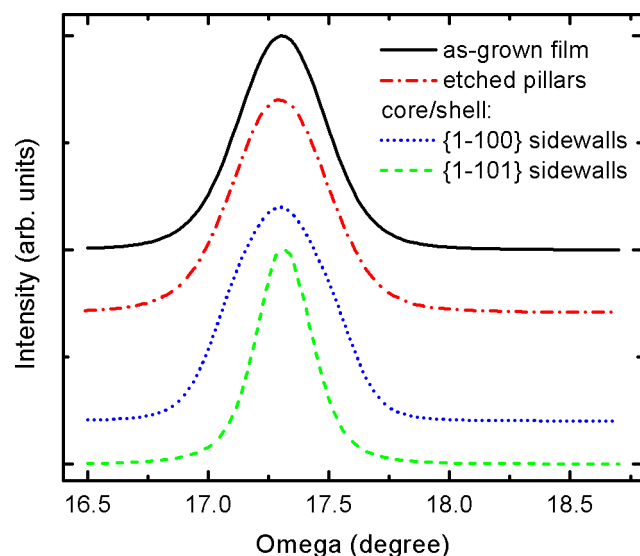


FIG. 4. Comparison of X-ray rocking curves (0002) for epilayer film, ICP-etched pillars, and overgrown shells with semi-polar $\{1\bar{1}01\}$ and non-polar $\{1\bar{1}00\}$ sidewalls.

TABLE I. FWHM and peak intensity of (0002) reflection of as-grown GaN-on-Si epilayer, ICP-etched GaN pillars, and core-shell structures semi-polar $\{1\bar{1}01\}$ and non-polar $\{1\bar{1}00\}$ sidewalls.

	FWHM (deg)	Peak intensity (cps)
As-grown	0.407	1.5×10^7
Etched pillars	0.441	5×10^4
Shell, $\{1\bar{1}01\}$ sidewalls	0.409	4.8×10^5
Shell, $\{1\bar{1}00\}$ sidewalls	0.264	1.0×10^6

samples indicates significant improvement in the material quality relative to the starting epilayer. It is worth noting that the FWHM values of the overgrown samples combine contributions from both the poor crystalline quality cores and the dislocation-free shells. Although the reduction of dislocation density in the semi-polar shells has been demonstrated, the dislocation-free region is mostly confined to the upper section of the overgrown shell where the shell thickness is small, whereas the bottom thick part of the shell still contains laterally propagating dislocations.^{7,18} In contrast, for non-polar shells, the thickness of the dislocation-free shell region is higher.

Material quality and the level of strain relaxation of the GaN pillars and core-shell structures at different stages of processing have been assessed by room-temperature PL, Raman, and CL spectroscopy. PL spectra of 2 μm diameter GaN pillars (cores) as well as overgrown shells obtained at 950 °C are shown in Fig. 5(a). The dotted vertical lines in Fig. 5 denote the peak energy positions of the near-band edge (NBE) PL and Raman E_2^H phonon mode measured for a free-standing 3 mm thick GaN commercial sample grown by HVPE. The significant red-shift of the NBE peak of etched pillars compared to the bulk-like thick GaN is due to in-plane biaxial tensile strain caused by lattice and thermal expansion mismatch between GaN and Si. However, compared to the initial thin film (not shown), significant strain-relaxation has been observed in the etched pillars.¹⁹ Notably, a broad PL band around 2.2 eV observed in the ICP-etched pillars has been significantly reduced after shell overgrowth, particularly for the shells grown on PA-etched pillars. It is well recognized that this band, often referred to as yellow luminescence (YL), is caused by defects and/or impurities whose nature is still being actively debated in the literature.^{20,21} Decreasing the YL intensity with respect to the NBE emission indicates a superior quality of the overgrown GaN shells as compared to the initial material. In general, despite the difference in morphology, core-shell structures with semipolar and non-polar sidewalls exhibit very similar optical properties that are also similar to those of the shells grown at 1000 °C (not shown).

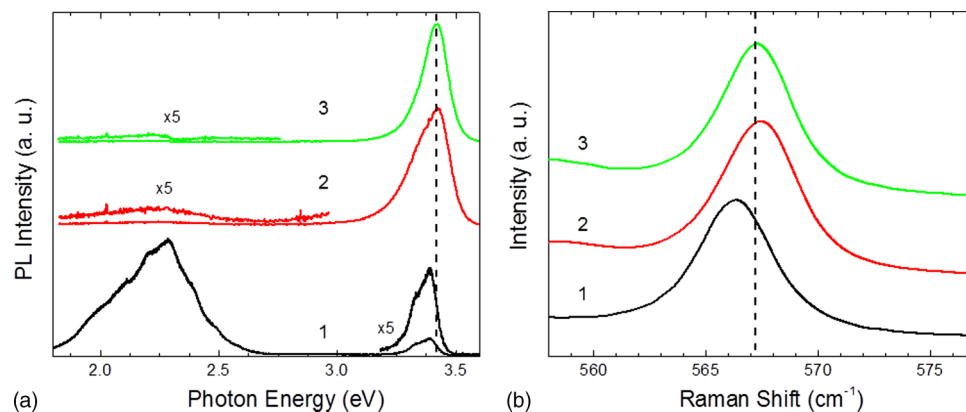


FIG. 5. Room-temperature (a) PL and (b) Raman scattering spectra of—(1) ICP-etched pillars and core-shell structures with (2) semipolar and (3) non-polar sidewalls grown at 950 °C. Vertical dotted lines denote NBE and E_2^H peak positions measured for bulk HVPE GaN, 3.42 eV and 567.2 cm^{-1} , respectively.

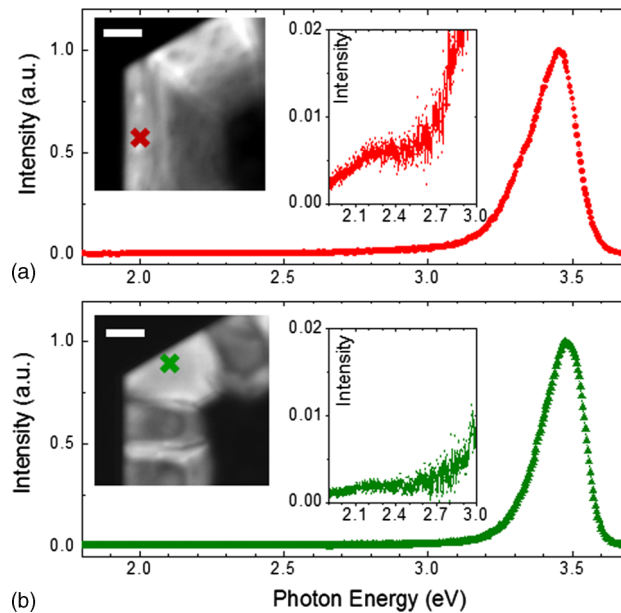


FIG. 6. CL spectra of the GaN shells grown at 950 °C on (a) ICP-etched and (b) PA-etched pillars. Positions of the irradiating electron beam are marked in the corresponding panchromatic CL images (left insets). YL bands are enhanced in the right insets. Scale bars correspond to 500 nm.

Raman scattering spectra of GaN pillars and core-shell structures taken in the vicinity of the E_2^H phonon mode are plotted in Fig. 5(b). Partial strain relaxation is observed in all ICP-etched pillars as compared to the thin film (not shown), which is consistent with the PL data.¹⁹ After the GaN shell growth, further strain relaxation is evident from the shifting of the E_2^H peak toward the bulk value. Thus, the overgrowth produces essentially strain-free material of high optical quality.

Fig. 6 shows local CL spectra obtained on individual GaN shells. Use of an electron acceleration voltage of 5 kV (penetration depth is ≈ 160 nm, see Fig. S5) ensures that only the overgrown GaN is probed. The CL data are in a good agreement with the PL spectra collected over the large sampling areas. The primary CL peak around 3.46 eV is assigned to NBE emission while the YL is very weak. The NBE peak intensity of the PA-etched sample was found 3- to 5-fold higher than that of the ICP-etched sample. The NBE peak of the PA-etched sample is narrower than that of the ICP-etched sample in the normalized CL spectra in Fig. 6, which is in agreement with PL data.

In conclusion, large-area arrays of vertically aligned GaN core-shell structures have been fabricated using selective epitaxial overgrowth of GaN pillars obtained by top-down etching of GaN-on-Si epilayers. We show that the facets of GaN shells can be switched from $\{1\bar{1}01\}$ semi-polar to $\{1\bar{1}00\}$ non-polar planes by employing a hot phosphoric acid etching of GaN pillars prior to the overgrowth by HVPE and tuning the growth temperature. XRD reveals improved crystal quality of the overgrown shells as compared to the initial GaN cores. Room-temperature PL and CL spectra exhibit significant enhancement of the NBE peak in core-shell structures as compared to both the starting epilayer and etched cores with significant reduction in yellow luminescence. In addition, significant in-plane strain relaxation is observed after the shell overgrowth. The results demonstrate the effectiveness of combining the scalability and reproducibility of top-down techniques with the high material quality achievable using selective homoepitaxial overgrowth to form GaN core-shell structures. Such structures have the potential to be utilized for large-area photodetectors, emitters, and photovoltaic devices, and could be a major enabler of the GaN-on-Si technology.

GaN pillars were fabricated at the Nanofab clean room of the NIST Center for Nanoscale Science and Technology. The University of Maryland portion of the work was partially supported by the Defense Threat Reduction Agency, Basic Research Award # HDTRA1-10-1-0107. H. P. Y. acknowledges support under the Cooperative Research Agreement between the University of Maryland and the NIST Center for Nanoscale Science and Technology, award 70NANB10H193.

- ¹ S. Li and A. Waag, *J. Appl. Phys.* **111**, 071101 (2012).
- ² P. Waltereit, O. Brandt, A. Trampert, H. Grahn, J. Menniger, M. Ramsteiner, M. Reiche, and K. H. Ploog, *Nature* **406**, 865 (2000).
- ³ W. Bergbauer, M. Strassburg, Ch. Kölper, N. Linder, C. Roder, J. Lähnemann, A. Trampert, S. Fündling, S. F. Li, H.-H. Wehmann, and A. Waag, *Nanotechnology* **21**, 305201 (2010).
- ⁴ K. A. Bertness, A. W. Sanders, D. M. Rourke, T. E. Harvey, A. Roshko, J. B. Schlager, and N. A. Sanford, *Adv. Funct. Mater.* **20**, 2911 (2010).
- ⁵ N. A. Fichtenbaum, C. J. Neufeld, C. Schaake, Y. Wu, M. H. Wong, M. Grundmann, S. Keller, S. P. Denbaars, J. S. Speck, and U. K. Mishra, *Jpn. J. Appl. Phys., Part 2* **46**, L230 (2007).
- ⁶ E. D. Le Boulbar, I. Gîrgel, C. J. Lewins, P. R. Edwards, R. W. Martin, A. Šatka, D. W. E. Allsopp, and P. A. Shields, *J. Appl. Phys.* **114**, 094302 (2013).
- ⁷ S. Krylyuk, D. Paramanik, M. King, A. Motayed, J.-Y. Ha, J. E. Bonevich, A. Talin, and A. V. Davydov, *Appl. Phys. Lett.* **101**, 241119 (2012).
- ⁸ Certain commercial equipment instruments or materials are identified in this paper to foster understanding. Such identification does not imply recommendation or endorsement by the National Institute of Standards and Technology nor does it imply that the materials or equipment identified are necessarily the best available for the purpose.
- ⁹ D. Paramanik, A. Motayed, G. S. Aluri, J.-Y. Ha, S. Krylyuk, A. V. Davydov, M. King, S. McLaughlin, S. Gupta, and H. Cramer, *J. Vac. Sci. Technol. B* **30**, 052202 (2012).
- ¹⁰ D. Zhuang and J. H. Edgar, *Mater. Sci. Eng. R* **48**, 1 (2005).
- ¹¹ L. Chen, Y. Huang, J. Chen, Y. Sun, T. Li, D.-G. Zhao, and H. Gong, *Proc. SPIE* **6621**, 66211A (2008).
- ¹² T. Ide, M. Shimizu, A. Suzuki, X.-Q. Shen, H. Okumura, and T. Nemoto, *Jpn. J. Appl. Phys., Part 1* **40**, 4785 (2001).
- ¹³ H.-P. Liu, J.-D. Tsay, W.-Y. Liu, Y.-D. Guo, J. T. Hsu, and I.-G. Chen, *J. Cryst. Growth* **260**, 79 (2004).
- ¹⁴ A. Lundskog, U. Forsberg, P. O. Holtz, and E. Janzen, *Cryst. Growth Des.* **12**, 5491 (2012).
- ¹⁵ See supplementary material at <http://dx.doi.org/10.1063/1.4899296> for additional SEM images of GaN core-shell structures.
- ¹⁶ Y. Kaneko, N. Yamada, T. Takeuchi, Y. Yamaoka, H. Amano, and I. Akasaki, *Solid-State Electron.* **41**, 295 (1997).
- ¹⁷ D. Du, D. J. Srolovitz, M. E. Coltrin, and C. C. Mitchell, *Phys. Rev. Lett.* **95**, 155503 (2005).
- ¹⁸ S. Tanaka, Y. Kawaguchi, N. Sawaki, M. Hibino, and K. Hiramatsu, *Appl. Phys. Lett.* **76**, 2701 (2000).
- ¹⁹ R. Debnath, J.-Y. Ha, B. Wen, D. Paramanik, A. Motayed, M. R. King, and A. V. Davydov, *J. Vac. Sci. Technol. B* **32**, 021204 (2014).
- ²⁰ M. A. Reshchikov and H. Morkoç, *J. Appl. Phys.* **97**, 061301 (2005).
- ²¹ D. O. Demchenko, I. C. Diallo, and M. A. Reshchikov, *Phys. Rev. Lett.* **110**, 087404 (2013).

Faceting Control in Core-Shell GaN micropillars using Selective Epitaxy

Sergiy Krylyuk,^{1,2} Ratan Debnath,^{1,3} Heayoung P. Yoon,^{4,5} Matthew R. King,⁶

Jong-Yoon Ha,^{1,2} Baomei Wen,^{1,3} Abhishek Motayed,^{1,2} and Albert V. Davydov¹

¹ *Materials Science and Engineering Division, National Institute of Standards and Technology,
Gaithersburg, Maryland 20899, USA*

² *Institute for Research in Electronics and Applied Physics, University of Maryland, College
Park, Maryland 20742, USA*

³ *N5 Sensors Inc., Rockville, Maryland 20852, USA*

⁴ *Center for Nanoscale Science and Technology, National Institute of Standards and Technology,
Gaithersburg, Maryland 20899, USA*

⁵ *Maryland Nanocenter, University of Maryland, College Park, Maryland 20742, USA*

⁶ *Northrop Grumman ES, Linthicum, Maryland 21090, USA*

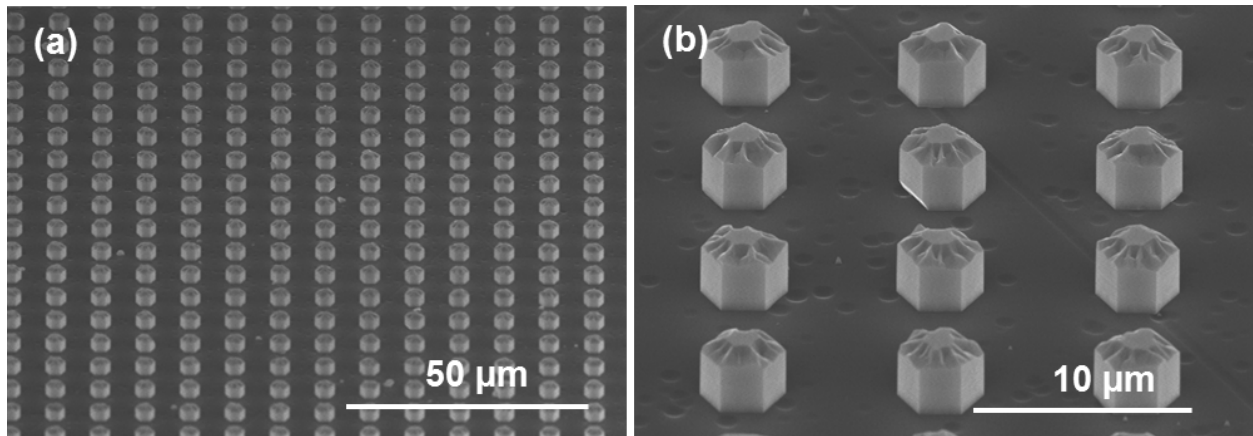


FIG. S1. Tilted SEM images of GaN shells grown on PA-etched GaN/Si pillars at 950 °C for 2 min.

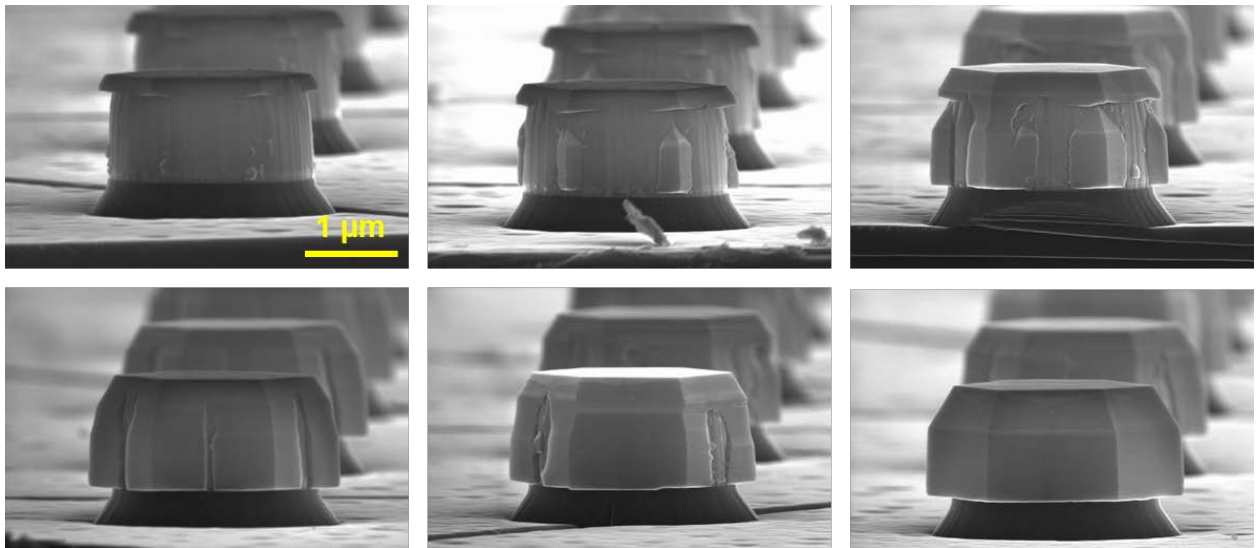


FIG. S2. SEM images showing shell formation on ICP-etched pillars at 950 °C. All images were taken on the same sample overgrown for 1 min. Pillars with incomplete shells are found around the edges of an array where the growth rate is lower. The scale bar applies to all images.

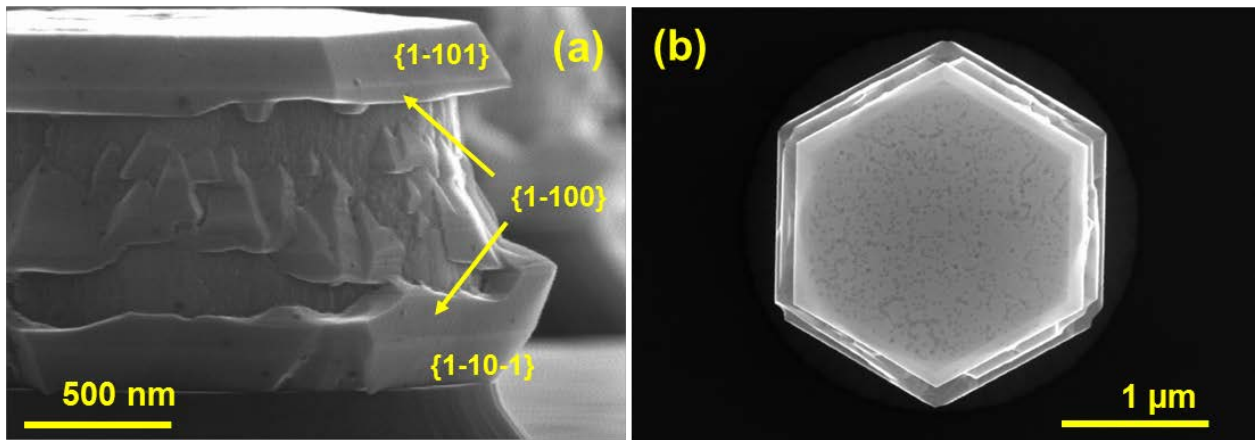


FIG. S3. Side- and top-view of GaN shells grown on PA-etched pillars at 950 °C for 30 s.

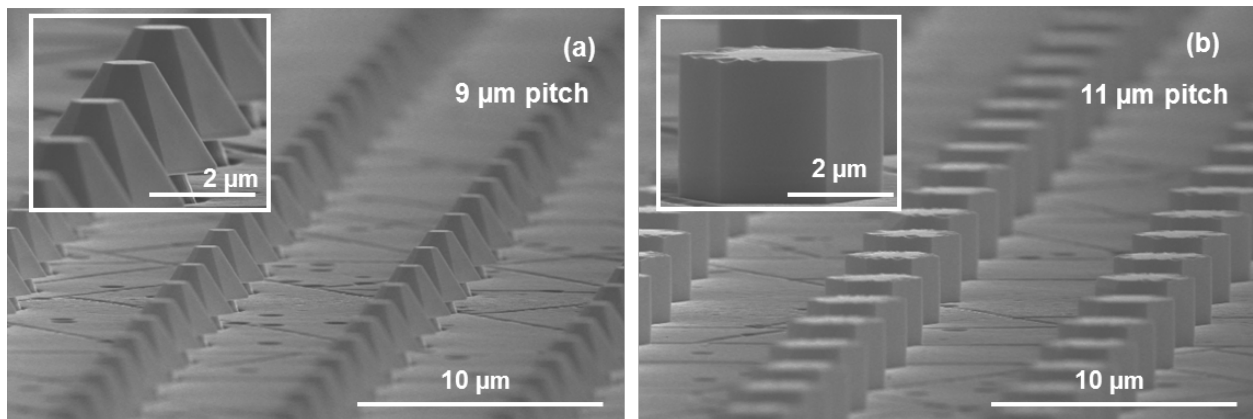


FIG. S4. GaN shells with (a) semipolar and (b) nonpolar sidewalls grown on adjacent arrays of PA-etched pillars with different pitch as indicated. $T_{\text{growth}} = 950 \text{ }^\circ\text{C}$.

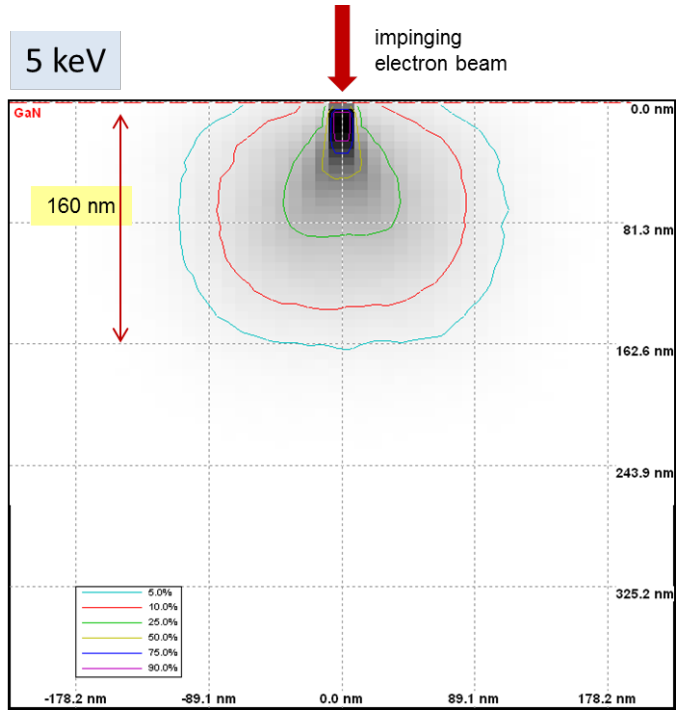


Figure S5. Carrier generation depth in GaN at an electron acceleration voltage of 5 kV as calculated by Monte Carlo simulation [after P. Hovington, D. Drouin, and R. Gauvin, *Scanning* **19**, 1 (1997).]